Computer Assisted Mechanics and Engineering Sciences, 8: 409–424, 2001.


# A Trefftz patch recovery method for smooth stress resultants and applications to Reissner–Mindlin equilibrium plate models

Edward A.W. Maunder
*School of Engineering and Computer Science, University of Exeter*
*Exeter, EX4 4QF, England*

(Received June 30, 2000)

A method is proposed for smoothing approximate fields of stress-resultants in patches of finite elements. The method is based on combining Trefftz fields of stress-resultants in a $p$-version so as to obtain a closest fit using the strain energy norm as a measure. The local systems of equations are formulated from boundary integrals. The method is applied to a problem of a square plate modelled by hybrid equilibrium plate elements using Reissner–Mindlin theory. Results for the problem indicate that the smooth solution for stresses can be in close agreement with the analytic solution in the interior of a patch. Proposals are also included to aid the visualization of tensor and vector continuous fields as stress trajectories.

## 1. Introduction

As noted in [10, 15] many methods have been proposed for post-processing stress fields derived from finite element models. Most have been directed towards the more conventional conforming models where stress fields are generally neither statically admissible nor continuous. The usual aim is to improve stress quality by local or global procedures for stress smoothing with two purposes in mind: (a) to provide a better reference solution for estimating error in adaptive procedures, and/or (b) to improve reliability of design. Stress fields from equilibrium models may be statically admissible, but not necessarily continuous, and so again smoothing may be desirable.

Smoothing methodologies are often based on fitting polynomial stress fields by a least squares fit with discrete values, taking each stress component separately. It is proposed in this paper to fit local stress fields by minimising the strain energy of the difference between a stress field which is both statically and kinematically admissible within a patch, i.e. a Trefftz solution, and the finite element stress field.

The Trefftz patch recovery (TPR) process for obtaining smooth stress-resultants is presented in Section 2 when the initial stress-resultant field is obtained from a general finite element model but with special consideration of equilibrating or conforming fields. A hierarchical adaptive procedure is described in Section 3 for application to plate problems governed by Reissner–Mindlin theory. An illustrative problem of a square plate representing a reinforced concrete slab as a bridge deck is presented in Section 4. In this problem stress concentrations exist due to boundary layer effects [14], and initial stress-resultants are derived from equilibrium models. Section 5 proposes refined methods for constructing stress-resultant trajectories to aid the visualization of smoothed fields.

## 2. Trefftz patch recovery of stress-resultants

Stress fields are considered within a patch $\Delta$ of elements in which the stresses derived from a finite element analysis are denoted by $\sigma_{\mathrm{FE}}$. These stresses may satisfy certain conditions, such as those of kinematic or static admissibility when derived from a conforming or an equilibrium finite element

model respectively. On the other hand neither of these conditions may be satisfied. In any event, the stresses $\sigma_{\mathrm{FE}}$ are generally not fully continuous. The aim with Trefftz recovery is to define within a patch continuous stresses $\tilde{\sigma}$ which satisfy all the linear elastic equations whilst remaining close to $\sigma_{\mathrm{FE}}$. One way to achieve this aim is to minimize $\mathbf{E} = \|\tilde{\sigma} - \sigma_{\mathrm{FE}}\|_{\mathrm{E}}$ over a patch, where $\mathbf{E}$ refers to the strain energy norm [14].

To this end, a vector space $\mathbf{Tr}$ is defined which is comprised of homogeneous Trefftz stress fields $\tilde{\sigma}_1$, so that $\tilde{\sigma}$ can be expressed as in Eq. (1).

$$\{\tilde{\sigma}\} = \{\tilde{\sigma}_1\} + \{\tilde{\sigma}_0\}, \qquad \text{where} \quad \{\tilde{\sigma}_1\} = [H]\{\beta\}. \tag{1}$$

The columns of $[H]$ contain a basis for $\mathbf{Tr}$, $\{\beta\}$ contains stress parameters to be determined, and $\{\tilde{\sigma}_0\}$ contains a particular Trefftz solution for stresses which is in equilibrium with loads distributed within the domain of a patch. Then $\mathbf{E}$ can be expressed as in Eq. (2),

$$\begin{aligned}
\mathbf{E} &= \frac{1}{2}\int_\Omega \{\tilde{\sigma}_1 + \tilde{\sigma}_0 - \sigma_{\mathrm{FE}}\}^T [f]\{\tilde{\sigma}_1 + \tilde{\sigma}_0 - \sigma_{\mathrm{FE}}\}\,\mathrm{d}\Omega \\
&= \frac{1}{2}\int_\Omega \{\tilde{\sigma}_1 + \tilde{\sigma}_0 - \sigma_{\mathrm{FE}}\}^T \{\tilde{\varepsilon}_1 + \tilde{\varepsilon}_0 - \varepsilon_{\mathrm{FE}}\}\,\mathrm{d}\Omega \\
&= \tilde{U}_1 + \tilde{U}_0 + U_{\mathrm{FE}} + \int_\Omega \left(\{\tilde{\sigma}_0\}^T\{\tilde{\varepsilon}_1\} - \{\sigma_{\mathrm{FE}}\}^T\{\tilde{\varepsilon}_1\} - \{\sigma_{\mathrm{FE}}\}^T\{\tilde{\varepsilon}_0\}\right)\mathrm{d}\Omega \\
&= \tilde{U}_1 - \int_\Omega \{\sigma_{\mathrm{FE}} - \tilde{\sigma}_0\}^T\{\tilde{\varepsilon}_1\}\,\mathrm{d}\Omega + \left(\tilde{U}_0 + U_{\mathrm{FE}} - \int_\Omega \{\sigma_{\mathrm{FE}}\}^T\{\tilde{\varepsilon}_0\}\,\mathrm{d}\Omega\right)
\end{aligned} \tag{2}$$

due to the symmetry of the flexibility matrix $[f]$ which represents the constitutive relations. As a function of $\{\beta\}$, $\mathbf{E}$ is re-expressed as

$$\mathbf{E} = \frac{1}{2}\{\beta\}^T[\tilde{F}]\{\beta\} - \{\beta\}^T \int_\Omega [H]^T[f]\{\sigma_{\mathrm{FE}} - \tilde{\sigma}_0\}\,\mathrm{d}\Omega + (\text{constants}).$$

Minimization of $\mathbf{E}$ for a linear elastic domain is accomplished by solving Eq. (3),

$$[\tilde{F}]\{\beta\} = \{\delta\}, \qquad \text{where} \quad [\tilde{F}] = \int_\Delta [H]^T[f][H]\,\mathrm{d}\Omega \quad \text{and} \quad \{\delta\} = \int_\Delta [H]^T[f]\{\sigma_{\mathrm{FE}} - \tilde{\sigma}_0\}\,\mathrm{d}\Omega. \tag{3}$$

After the minimization,

$$\{\beta\}^T\{\delta\} = \{\beta\}^T[\tilde{F}]\{\beta\} = 2\tilde{U}_1,$$

and then $\mathbf{E}$ is given by Eq. (4),

$$\begin{aligned}
\mathbf{E} &= U_{\mathrm{FE}} + \left(\tilde{U}_0 - \int_\Omega \{\sigma_{\mathrm{FE}}\}^T\{\tilde{\varepsilon}_0\}\,\mathrm{d}\Omega\right) - \tilde{U}_1, \qquad \text{or} \\
&= U_{\mathrm{FE}} - \tilde{U}_1 \quad \text{in the absence of lateral load.}
\end{aligned} \tag{4}$$

Equations (3) and (4) are now considered for particular cases of finite element models.

### 2.1. $\sigma_{\mathrm{FE}}$ is statically admissible

Since $\{\sigma_{\mathrm{FE}} - \tilde{\sigma}_0\}$ is now in equilibrium with zero lateral loads,

$$\begin{aligned}
&\int_\Omega \{\sigma_{\mathrm{FE}} - \tilde{\sigma}_0\}^T\{\tilde{\varepsilon}_1\}\,\mathrm{d}\Omega = \oint_{\partial\Omega} \{\hat{t} - \tilde{t}_0\}^T\{\tilde{u}_1\}\,\mathrm{d}\Gamma = \{\beta\}^T \oint_{\partial\Omega} [\bar{N}]^T\{\hat{t} - \tilde{t}_0\}\,\mathrm{d}\Gamma, \\
&\{\delta\} = \oint_{\partial\Omega} [\bar{N}]^T\{\hat{t} - \tilde{t}_0\}\,\mathrm{d}\Gamma.
\end{aligned} \tag{5}$$

Thus $\{\delta\}$ transforms to a form involving only contour integrals as in Eq. (5), where $\{\hat{t}\}$ and $\{\tilde{t}_0\}$ represent boundary tractions in equilibrium with $\sigma_{\mathrm{FE}}$ and $\tilde{\sigma}_0$ respectively, and the basis for **Tr** leads to corresponding displacements on the boundary defined by $\{\tilde{u}\} = [\bar{N}]\{\beta\}$. The latter displacements are defined to within rigid body movements. The definition of displacements can of course be extended to cover the whole patch, leading to displacement and strain fields $\{\tilde{u}\} = [N]\{\beta\}$ and $\{\tilde{\varepsilon}\} = [B]\{\beta\}$. In this case Eq. (3) takes on the form of weak equilibrium equations for a displacement element representing the whole patch. $\{\delta\}$ corresponds to the generalised forces consistent with the self-balancing boundary tractions $\{\hat{t} - \tilde{t}_0\}$, and $[\tilde{F}]$ has the form of the stiffness matrix in Eq. (6),

$$[\tilde{F}] = \int_{\Delta} [B]^T [f]^{-1} [B] \, \mathrm{d}\Omega. \tag{6}$$

The strain energy of the stress solution $[H]\{\beta\}$ is thus a lower bound to the strain energy of this traction driven problem, and it is thus to be expected that the strain energy of $[H]\{\beta\}$ will increase as the space **Tr** is enlarged in dimension. The general expression for **E** in Eq. (4) can be re-expressed as in Eq. (7),

$$\mathbf{E} = U_{\mathrm{FE}} + \left( \tilde{U}_0 - \int_{\Omega} \omega \cdot \tilde{u}_0 \, \mathrm{d}\Omega - \oint_{\partial\Omega} \{\hat{t}\}^T \{\tilde{u}_0\} \, \mathrm{d}\Gamma \right) - \tilde{U}_1 \,. \tag{7}$$

In Eq. (7), the product $\omega \cdot \tilde{u}_0$ refers to the work done by lateral loads $\omega$ moving through the lateral deflection component of $\tilde{u}_0$. It remains to be seen whether **E** can form a useful local error measure for the patch.

### 2.2. $\sigma_{\mathrm{FE}}$ is kinematically admissible

In this case,

$$\begin{aligned} &\int_{\Omega} \{\sigma_{\mathrm{FE}} - \tilde{\sigma}_0\}^T \{\tilde{\varepsilon}_1\} \, \mathrm{d}\Omega = \int_{\Omega} \{\tilde{\sigma}_1\}^T \{\varepsilon_{\mathrm{FE}} - \tilde{\varepsilon}_0\} \, \mathrm{d}\Omega = \{\beta\}^T \oint_{\partial\Omega} [\bar{T}]^T \{u_{\mathrm{FE}} - \tilde{u}_0\} \, \mathrm{d}\Gamma, \\ &\{\delta\} = \oint_{\partial\Omega} [\bar{T}]^T \{u_{\mathrm{FE}} - \tilde{u}_0\} \, \mathrm{d}\Gamma, \end{aligned} \tag{8}$$

where $\{u_{\mathrm{FE}}\}$ and $\{\tilde{u}_0\}$ represent boundary displacements compatible with $\sigma_{\mathrm{FE}}$ and $\tilde{\sigma}_0$ respectively, and the basis for **Tr** leads to corresponding tractions on the boundary defined by $\{\tilde{t}_1\} = [\bar{T}]\{\beta\}$. Equation (3) now takes the form of weak compatibility equations for a stress based equilibrium element representing the whole patch. $[\tilde{F}]$ has the form of a flexibility matrix, and for this displacement driven problem, the strain energy of the stress solution $[H]\{\beta\}$ is again a lower bound. After minimization of **E**, its form can be given by Eq. (9),

$$\mathbf{E} = U_{\mathrm{FE}} + \left( \tilde{U}_0 - \int_{\Omega} \omega \cdot u_{\mathrm{FE}} \, \mathrm{d}\Omega - \oint_{\partial\Omega} \{\tilde{t}_0\}^T \{u_{\mathrm{FE}}\} \, \mathrm{d}\Gamma \right) - \tilde{U}_1 \,, \tag{9}$$

where $\tilde{t}_0$ denotes particular tractions in equilibrium with stresses $\tilde{\sigma}_0$, and a distributed pressure load $\omega$.

### 2.3. $\sigma_{\mathrm{FE}}$ is a general stress field

Recent work by Debongnie and Beckers [1] has shown that a general approximate elastic stress field can be decomposed into two fields as in Eq. (10), one $\sigma_e$ which is hyperstatic (self-stressing), and one $\sigma_c$ which is kinematically admissible,

$$\sigma_{\mathrm{FE}} = \sigma_e + \sigma_c \,. \tag{10}$$

These fields belong to orthogonal complements of the stress space in a patch $\Omega$ which has entirely static boundary conditions. Then,

$$\sigma_{\mathrm{FE}} = \sigma_e + \sigma_c\,,$$

$$\int_\Omega \{\sigma_{\mathrm{FE}} - \tilde{\sigma}_0\}^T\{\tilde{\varepsilon}_1\}\,\mathrm{d}\Omega = \int_\Omega \{\sigma_e\}^T\{\tilde{\varepsilon}_1\} + \{\sigma_c - \tilde{\sigma}_0\}^T\{\tilde{\varepsilon}_1\}\,\mathrm{d}\Omega = \int_\Omega \{\sigma_c - \tilde{\sigma}_0\}^T\{\tilde{\varepsilon}_1\}\,\mathrm{d}\Omega$$

$$= \int_\Omega \{\tilde{\sigma}_1\}^T\{\varepsilon_c - \tilde{\varepsilon}_0\}\,\mathrm{d}\Omega = \{\beta\}^T \oint_{\partial\Omega} \{\tilde{t}_1\}^T\{u_c - \tilde{u}_0\}\,\mathrm{d}\Gamma,$$

where $u_c$ denotes a displacement field conforming with $\sigma_c$. In this case,

$$\{\delta\} = \oint_{\partial\Omega} [\bar{T}]^T\{u_c - \tilde{u}_0\}\,\mathrm{d}\Gamma. \tag{11}$$

The expression for $\mathbf{E}$ takes a similar form to that in Eq. (9), but with $u_{\mathrm{FE}}$ replaced by $u_c$.

Thus it can be seen that although the general aim is to recover smooth stresses in a patch, the Trefftz procedure has an hermaphroditic nature! Its "gender" depends on the nature of the problem. It should also be noted that in each case, $[\tilde{F}]$ can also be formulated from contour integration as in Eq. (12), which may simplify the computational aspects of Eq. (3),

$$[\tilde{F}] = \oint_{\partial\Delta} [\bar{N}]^T[\bar{T}]\,\mathrm{d}\Gamma. \tag{12}$$

## 3. Application to plates governed by Reissner–Mindlin theory

### 3.1. Generation of a basis for a 'Tr' space

Stress fields are now interpreted as moment fields, and a basis for $\mathbf{Tr}$ can be generated from two scalar rotation functions $g$ and $f$ [7]. The rotations $\theta$ of a normal to the plate are defined in Eq. (13),

$$\lfloor\ \theta_x \quad \theta_y\ \rfloor = \lfloor\ -g_{,x} \quad -g_{,y}\ \rfloor \quad \text{and/or} \quad \lfloor\ f_{,y} \quad -f_{,x}\ \rfloor\,. \tag{13}$$

The differential equations of equilibrium lead to the biharmonic and/or the "negative" Helmholtz equations as expressed in Eq. (14),

$$\nabla^4 g = 0 \qquad \text{and/or} \qquad \nabla^2 f = \frac{10}{h^2}\cdot f, \tag{14}$$

where $h$ is the plate thickness. In the present paper, these rotation functions will be restricted to polynomials of finite degree, and hence Trefftz type solutions generated by the negative Helmholtz equation are excluded.

In terms of $g$, the transverse deflections $w$ can be derived to within rigid body movements as in Eq. (15),

$$w = g - \frac{h^2}{5(1-\nu)}\cdot\nabla^2 g. \tag{15}$$

Components of moments and shear forces are derived as in Eq. (16),

$$\begin{Bmatrix} m_x \\ m_y \\ m_{xy} \end{Bmatrix} = -D\begin{bmatrix} 1 & \nu & 0 \\ \nu & 1 & 0 \\ 0 & 0 & \frac{1}{2}(1-\nu) \end{bmatrix}\begin{Bmatrix} g_{,xx} \\ g_{,yy} \\ 2g_{,xy} \end{Bmatrix},$$

$$\begin{Bmatrix} q_x \\ q_y \end{Bmatrix} = -\frac{h^2}{5(1-\nu)}\cdot\mathrm{grad}(\nabla^2 g), \tag{16}$$

where $\nu$ and $D$ denote Poisson's ratio and the flexural rigidity of the plate respectively.

**Table 1.** A basis for Trefftz moments up to degree 4, and corresponding transverse shear forces

| Ref. No. | $m_x$ | $m_y$ | $m_{xy}$ | $q_x$ | $q_y$ |
|---|---|---|---|---|---|
| 1 | 1 | $\nu$ | 0 | 0 | 0 |
| 2 | $\nu$ | 1 | 0 | 0 | 0 |
| 3 | 0 | 0 | 1 | 0 | 0 |
| 4 | $x$ | $-x$ | $-y$ | 0 | 0 |
| 5 | $-y$ | $y$ | $-x$ | 0 | 0 |
| 6 | $x$ | $\nu x$ | 0 | 1 | 0 |
| 7 | $\nu y$ | $y$ | 0 | 0 | 1 |
| 8 | $(-x^2+y^2)$ | $(x^2-y^2)$ | $2xy$ | 0 | 0 |
| 9 | $-2xy$ | $2xy$ | $(-x^2+y^2)$ | 0 | 0 |
| 10 | $(x^2-\nu y^2)$ | $\nu x^2-y^2$ | 0 | $2x$ | $-2y$ |
| 11 | $2(1+\nu)xy$ | $2(1+\nu)xy$ | $(1-\nu)(x^2+y^2)$ | $4y$ | $4x$ |
| 12 | $(-x^3+3xy^2)$ | $(x^3-3xy^2)$ | $(3x^2y-y^3)$ | 0 | 0 |
| 13 | $(-3x^2y+y^3)$ | $(3x^2y-y^3)$ | $(-x^3+3xy^2)$ | 0 | 0 |
| 14 | $\nu x^3+3(1-2\nu)xy^2$ | $x^3-3(2-\nu)xy^2$ | $(1-\nu)(3x^2y-2y^3)$ | $3(x^2-y^2)$ | $-6xy$ |
| 15 | $-3(2-\nu)x^2y+y^3$ | $3(1-2\nu)x^2y+\nu y^3$ | $(1-\nu)(-2x^3+3xy^2)$ | $-6xy$ | $3(-x^2+y^2)$ |
| 16 | $(x^4-6x^2y^2+y^4)$ | $-(x^4-6x^2y^2+y^4)$ | $4(-x^3y+xy^3)$ | 0 | 0 |
| 17 | $(x^3y-xy^3)$ | $(-xy^3+xy^3)$ | $(x^4-6x^2y^2+y^4)/4$ | 0 | 0 |
| 18 | $(3-\nu)x^4$ $-6(1+\nu)x^2y^2$ $-(1-3\nu)y^4$ | $(-1+3\nu)x^4$ $-6(1+\nu)x^2y^2$ $-(-3+\nu)y^4$ | $-4(1-\nu)(x^3y+xy^3)$ | $8(x^3-3xy^2)$ | $8(-3x^2y+y^3)$ |
| 19 | $(x^3y-\nu xy^3)$ | $(\nu x^3y-xy^3)$ | $(1-\nu)(x^4-y^4)/4$ | $(3x^2y-y^3)$ | $(x^3-3xy^2)$ |

A complete set of biharmonic polynomials has been derived using complex variables and tabulated for degree $n$ up to $n=8$ [6]. With these functions the dimension of **Tr** is 3 when $n=2$ (constant moments), and it increases by 4 for each unit increase in $n$. Thus the dimension of **Tr** is $(4n-5)$ for $n \geq 2$. The same Trefftz functions appear as Airy stress functions in plane stress, and transverse deflections in plates governed by Kirchhoff plate theory.

As with the case of plane stress, an alternative approach to establishing this dimension can be illuminating as well as providing alternative means to generate the basis functions [8]. This approach focuses directly on the moment fields and their physical characteristics. Moment fields defined by complete polynomials up to degree $p$ form a vector space $\mathbf{M}^p$ with dimension $1.5(p+1)(p+2)$ in a similar way to plane stress fields [8]. In the case of plane stress, a Trefftz subspace of dimension $(4p+3)$ was created by imposing three sets of constraint equations: two sets from the equations of equilibrium $\operatorname{div}(\sigma)=0$, and one set from the equation of compatibility $\nabla^2(\sigma_x+\sigma_y)=0$. Now for moment fields three sets of constraint equations are also imposed on the coefficients of the polynomial terms: one set from the equilibrium equation (17),

$$m_{x,xx}+2m_{xy,xy}+m_{y,yy}=0, \tag{17}$$

**Table 2.** Trefftz deflections and rotations corresponding to the basis in Table 1; N.B. $\mu = (1-\nu)$, $\alpha = h^2/5\mu$, and all expressions should be divided by the flexural rigidity $D$

| Ref. No. | $w$ | $\theta_x$ | $\theta_y$ |
|---|---|---|---|
| 1 | $-x^2/2$ | $x$ | $0$ |
| 2 | $-y^2/2$ | $0$ | $y$ |
| 3 | $-xy/\mu$ | $y/\mu$ | $x/\mu$ |
| 4 | $(-x^3+3xy^2)/6\mu$ | $(x^2-y^2)/2\mu$ | $-xy/\mu$ |
| 5 | $(3x^2y-y^3)/6\mu$ | $-xy/\mu$ | $(-x^2+y^2)/2\mu$ |
| 6 | $(-x^3+6\alpha x)/6$ | $x^2/2$ | $0$ |
| 7 | $(-y^3+6\alpha y)/6$ | $0$ | $y^2/2$ |
| 8 | $(x^4-6x^2y^2+y^4)/12\mu$ | $(-x^3+3xy^2)/3\mu$ | $(3x^2y-y^3)/3\mu$ |
| 9 | $(x^3y-xy^3)/3\mu$ | $(-3x^2y+y^3)/3\mu$ | $(-x^3+3xy^2)/3\mu$ |
| 10 | $(-x^4+y^4)/12+\alpha x^2-\alpha y^2$ | $x^3/3$ | $-y^3/3$ |
| 11 | $(-x^3y-xy^3)/3+4\alpha xy$ | $(3x^2y+y^3)/3$ | $(x^3+3xy^2)/3$ |
| 12 | $(x^5-10x^3y^2+5xy^4)/20\mu$ | $(-x^4+6x^2y^2-y^4)/4\mu$ | $(x^3y-xy^3)/\mu$ |
| 13 | $(5x^4y-10x^2y^3+y^5)/20\mu$ | $(-x^3y+xy^3)/\mu$ | $(-x^4+6x^2y^2-y^4)/4\mu$ |
| 14 | $(-x^3y^2+xy^4)/2+\alpha x^3-3\alpha xy^2$ | $(3x^2y^2-y^4)/2$ | $x^3y-2xy^3$ |
| 15 | $(x^4y-x^2y^3)/2-3\alpha x^2y+\alpha y^3$ | $-2x^3y+xy^3$ | $(-x^4+3x^2y^2)/2$ |
| 16 | $(-x^6+15x^4y^2-15x^2y^4+y^6)/30\mu$ | $(0.2x^5-2x^3y^2+xy^4)/\mu$ | $(-x^4y+2x^2y^3-0.2y^5)/\mu$ |
| 17 | $-(x^5y+xy^5)/20\mu+x^3y^3/6\mu$ | $(5x^4y-10x^2y^3+y^5)/20\mu$ | $(x^5-10x^3y^2+5xy^4)/20\mu$ |
| 18 | $-(x^6-5x^4y^2-5x^2y^4-y^6)/10$ $+2\alpha(x^4-6x^2y^2+y^4)$ | $(0.6x^5-2x^3y^2-xy^4)$ | $(-x^4y-2x^2y^3+0.6y^5)$ |
| 19 | $(-x^5y+xy^5)/20+\alpha(x^4-y^4)/4$ | $(5x^4y-y^5)/20$ | $(x^5-5xy^4)/20$ |

which leads to a subspace $\mathbf{M}^p_{SA}$ of statically admissible moments having dimension

$$1.5(p+1)(p+2)-0.5p(p-1)=(p^2+5p+3);$$

and two sets from the compatibility equations (18),

$$\begin{aligned} -\nu m_{x,x}+m_{y,x}-(1+\nu)m_{xy,y}+\frac{h^2}{10}((m_x-m_y)_{,xyy}-m_{xy,xxy}+m_{xy,yyy})=0,\\ -\nu m_{y,y}+m_{x,y}-(1+\nu)m_{xy,x}+\frac{h^2}{10}((m_y-m_x)_{,xxy}+m_{xy,xxx}-m_{xy,xyy})=0, \end{aligned} \tag{18}$$

which leads to the Trefftz subspace of dimension $(p^2+5p+3)-p(p+1)=(4p+3)$. This dimension agrees with that of **Tr** when $n=(p+2)$ which is required for the biharmonic polynomials to generate moment fields of degree $p$.

A basis for **Tr** for moments up to degree 4 ($n=6$) is given in Table 1 together with the corresponding shear forces. It should be noted that when $p>1$, each set of 4 additional moment fields includes 2 which are free of transverse shear. The displacements which are derived from these kinematically admissible moments, to within rigid body movements, are listed in Table 2.

### 3.2. A particular Trefftz solution for a patch with uniformly distributed load $\omega$

When a uniformly distributed pressure load $\omega$ is applied in the positive $z$ direction, a particular Trefftz solution for moments and shears is given by Eq. (19),

$$\lfloor m \rfloor = \frac{-\omega}{4} \begin{bmatrix} y^2 + \nu x^2 & x^2 + \nu y^2 & 2(1-\nu)xy \end{bmatrix}, \qquad \lfloor q \rfloor = \frac{-\omega}{2} \begin{bmatrix} x & y \end{bmatrix}. \tag{19}$$

The corresponding rotations and deflections, assuming the cartesian origin to be stationary, are given in Eq. (20),

$$\lfloor \theta \rfloor = \frac{-\omega}{4D} \begin{bmatrix} xy^2 & x^2 y \end{bmatrix}, \qquad \text{and} \qquad w = \frac{\omega}{4D} \left( \frac{x^2 y^2}{2} - \frac{h^2}{5(1-\nu)} (x^2 + y^2) \right). \tag{20}$$

### 3.3. Formation of Trefftz smoothing equations using scalar products

It has been shown that the formation of Eq. (3) reduces to performing contour integration on the boundary of a patch. Each contour integral determines the virtual work done by boundary tractions and corresponding displacements summed along the perimeter. When these quantities are simple polynomial functions of a position parameter $s$ for each boundary segment, it is possible to express tractions and displacements in terms of dual modes. Then tractions and displacements for each segment are represented by vectors with dual bases, and work on a segment is quantified by their scalar product. No explicit integration is required.

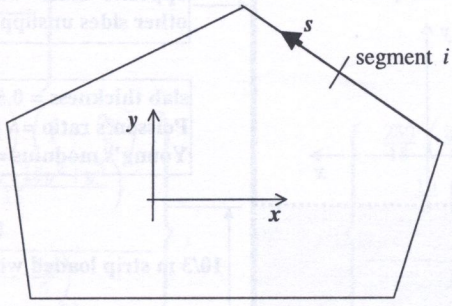


**Fig. 1.** Polygonal patch with a typical boundary segment

Figure 1 shows a general polygonal patch with local cartesian axes, and a typical boundary segment $i$ with a local ordinate $s$ having its origin at the midpoint. Dual bases for tractions and displacements can exploit orthogonal Legendre polynomials. Equation (3) can then be formed as in Eq. (21), for example when the patch is loaded by tractions,

$$\begin{aligned} [\tilde{F}] &= \sum_{\text{segment } i} [W_i]^T [Q_i] + [\Theta_{ni}]^T [M_{ni}] + [\Theta_{ti}]^T [M_{ti}], \\ \{\delta\} &= \sum_{\text{segment } i} [W_i]^T \{\hat{q}_{ni}\} + [\Theta_{ni}]^T \{\hat{m}_{ni}\} + [\Theta_{ti}]^T \{\hat{m}_{ti}\}. \end{aligned} \tag{21}$$

In this form all the matrices, before transposing, have dimensions $(p+1) \times (4p+3)$. $[W_i]$, $[\Theta_{ni}]$, and $[\Theta_{ti}]$ denote lateral deflections, normal and tangential components of rotations for segment $i$; $[Q_i]$, $[M_{ni}]$, and $[M_{ti}]$ denote shear, normal and torsional moments on segment $i$; and the vector quantities denote applied shear and moments to segment $i$.

Advantage has been taken of this way of constructing Eq. (3) in the examples presented in this paper which concern rectangular patches where the number of segments for the formation of $[\tilde{F}]$ is

just 4 (the number of sides). The pattern of $[\tilde{F}]$ is simplified in this case since the contributions to alternate submatrices cancel out as indicated in Eq. (22) when $p = 3$.

$$[\tilde{F}] = \left[\begin{array}{c|c|c|c} \tilde{F}_{11} & 0 & \tilde{F}_{13} & 0 \\ \hline 0 & \tilde{F}_{22} & 0 & \tilde{F}_{24} \\ \hline \tilde{F}_{31} & 0 & \tilde{F}_{33} & 0 \\ \hline 0 & \tilde{F}_{42} & 0 & \tilde{F}_{44} \end{array}\right] . \tag{22}$$

$[\tilde{F}]$ expands in an hierarchical way as the degree $p$ is increased, with 4 additional rows and columns being added to its border. When $p = 0$ (constant moments), $[\tilde{F}] = [\tilde{F}_{11}]$ and has dimension $3 \times 3$. This hierarchical form of $[\tilde{F}]$ may be exploited in an adaptive smoothing procedure where the degree $p$ is allowed to increase until convergence is satisfied according to some specified criterion [13].

## 4. SQUARE BRIDGE DECK

This example concerns a square bridge deck as specified in Figure 2, where unit value of Young's modulus is assumed for numerical simplicity, but the values of Poisson's ratio are generally appropriate for concrete. Three fields of equilibrating stress-resultants are considered for "smoothing". These fields are selected to illustrate that TPR explicitly smooths stresses and implicitly smooths any non-conformities which may be present in equilibrating fields.

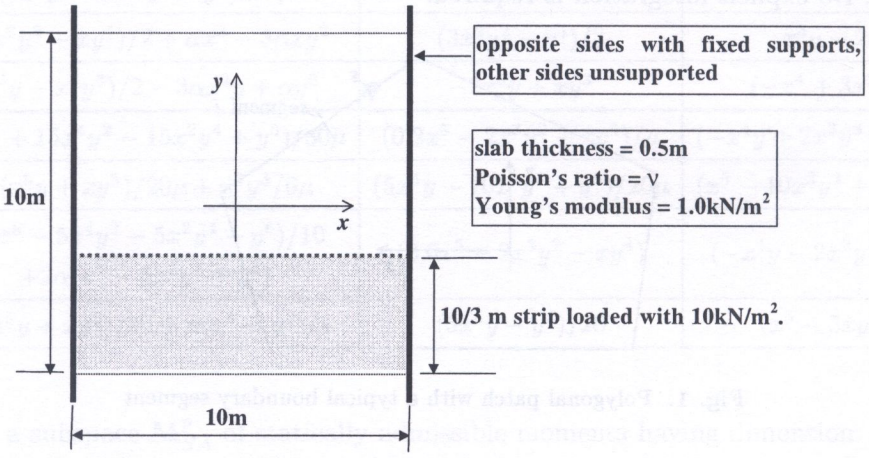


**Fig. 2.** Square bridge deck

This problem has been the subject of investigation as a benchmark problem [9], using dual finite element solutions based on hybrid equilibrium elements and 8-noded isoparametric conforming elements. An "analytic" reference solution has been approximated by a $48 \times 48$ mesh of conforming $p$-elements with degree 3.

The three fields of stress-resultants are defined: in a single beam strip with a width equal to the loaded width (field (i)); in families of orthogonal beam strips leading to a continuous field of stress-resultants throughout the slab (field (ii)); and in a $6 \times 6$ mesh of equilibrium finite elements as in [9] (field (iii)). The fields are discussed with reference to Figs. 3(a,b,c).

In all cases, the patch considered for smoothing is a square of side length 10/3 m, and this is shown shaded in Fig. 3. Field (i) is used with a Poisson's ratio equal to 0.0 when the field is also conforming, and equal to 0.2 when the field is non-conforming. The value of 0.2 is used with fields (ii) and (iii) which are also non-conforming. Non-conformities can be quantified by the residuals present in Eq. (18). Denoting this residual by the vector $r$, its norm is evaluated as in Eq. (23) taken over the

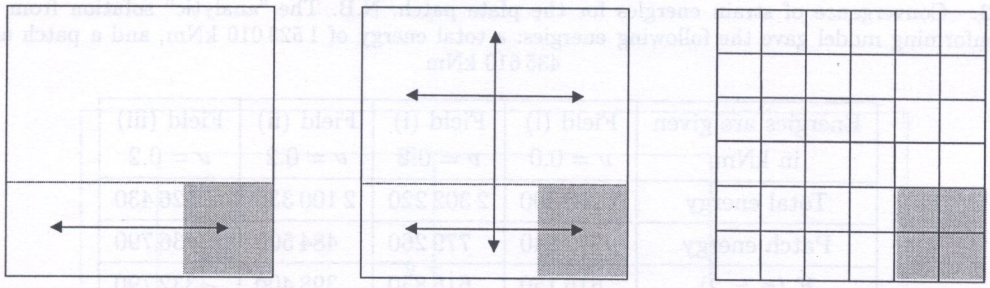

(a) (b) (c)

**Fig. 3.** Generation of fields of equilibrating stress-resultants

patch area. It should be noted that this term would be incomplete for the finite element field (iii), since it does not include terms representing the non-conformities between the elements [12].

$$\|r\| = \left( \int_{\Omega} \{r\}^T \{r\} \, \mathrm{d}\Omega \right)^{0.5} . \tag{23}$$

Fields (i) and (ii) are defined, as in the Hillerborg strip method [4], without torsional moment components. These are explicitly detailed in Eqs. (24) and (25) respectively,

$$\left\{ \begin{array}{c} m_x \\ m_y \\ \hline m_{xy} \\ \hline q_x \\ q_y \end{array} \right\} = \left\{ \begin{array}{c} \frac{250}{6}\left(\frac{3x^2}{25} - 1\right) \\ 0 \\ \hline 0 \\ \hline 10x \\ 0 \end{array} \right\} \quad \text{within the loaded strip,} \tag{24}$$

$$\left\{ \begin{array}{c} m_x \\ m_y \\ \hline m_{xy} \\ \hline q_x \\ q_y \end{array} \right\} = \left\{ \begin{array}{c} \frac{250}{18}\left(\frac{3x^2}{25} - 1\right)\left(1 - \frac{2y}{5}\right) \\ \frac{20}{6}\left(\frac{125+75y+15y^2+y^3}{15}\right) \\ \hline 0 \\ \hline \frac{10x}{3}\left(1 - \frac{2y}{5}\right) \\ \frac{20}{3}\left(\frac{25+10y+y^2}{10}\right) \end{array} \right\}, \quad \text{or} \quad \left\{ \begin{array}{c} \frac{250}{18}\left(\frac{3x^2}{25} - 1\right)\left(1 - \frac{2y}{5}\right) \\ \frac{10}{3}\left(\frac{125-15y^2+2y^3}{30}\right) \\ \hline 0 \\ \hline \frac{10x}{3}\left(1 - \frac{2y}{5}\right) \\ -\frac{10y}{3}\left(1 - \frac{y}{5}\right) \end{array} \right\}, \tag{25}$$

where the first vector occurs within the loaded strip, and the second vector occurs outside the loaded strip.

Stress-resultant and/or compatibility smoothing was carried out with the Trefftz biharmonic degree $n$ increased from 2 to 5. The energy results are tabulated in Table 3.

The convergence of the relative energy difference as defined by $\mathbf{E}/U_{\mathrm{FE}}$ is shown in Fig. 4 where part (b) is an enlarged view of the lower area of part (a). In this Figure, the lines labelled Series 1 to 4 refer to the results of smoothing field (i) when $\nu = 0.0$; field (i) when $\nu = 0.2$; and fields (ii) and (iii) when $\nu = 0.2$ in that order.

For field (i), stress-resultants are continuous within the beam strip and the patch, but discontinuous for the whole slab. However, when $\nu = 0.0$, the field conforms within the patch and since moments are quadratic, the Trefftz solution is identical with the field for $n \geq 4$. Hence this case also formed a valuable check for the Trefftz smoothing program.

For field (i), $\nu = 0.2$, the field does not conform and $\|r\| = 23.13$ kN. The Treftz solutions converge towards a different field of equilibrating stress-resultants which do conform.

For field (ii), the solution is improved with respect to energies, and this field is continuous throughout the slab but does not conform, and $\|r\| = 82.66$ kN. The Trefftz solutions again converge from below towards another equilibrating solution. It should be noted that fields (i) and (ii) lead

**Table 3.** Convergence of strain energies for the plate patch. N.B. The "analytic" solution from the fine mesh conforming model gave the following energies: a total energy of 1 523 010 kNm, and a patch energy of 435 610 kNm

| Energies are given in kNm | Field (i) $\nu = 0.0$ | Field (i) $\nu = 0.2$ | Field (ii) $\nu = 0.2$ | Field (iii) $\nu = 0.2$ |
|---|---|---|---|---|
| Total energy | 2 288 890 | 2 302 220 | 2 100 330 | 1 526 430 |
| Patch energy | 772 840 | 779 260 | 484 500 | 436 790 |
| **E** $(n = 2)$ | 616 150 | 616 830 | 398 400 | 332 790 |
| **E** $(n = 3)$ | 37 820 | 46 410 | 49 260 | 46 990 |
| **E** $(n = 4)$ | 0 | 14 170 | 14 080 | 6 640 |
| **E** $(n = 5)$ | 0 | 12 330 | 12 080 | 5 100 |

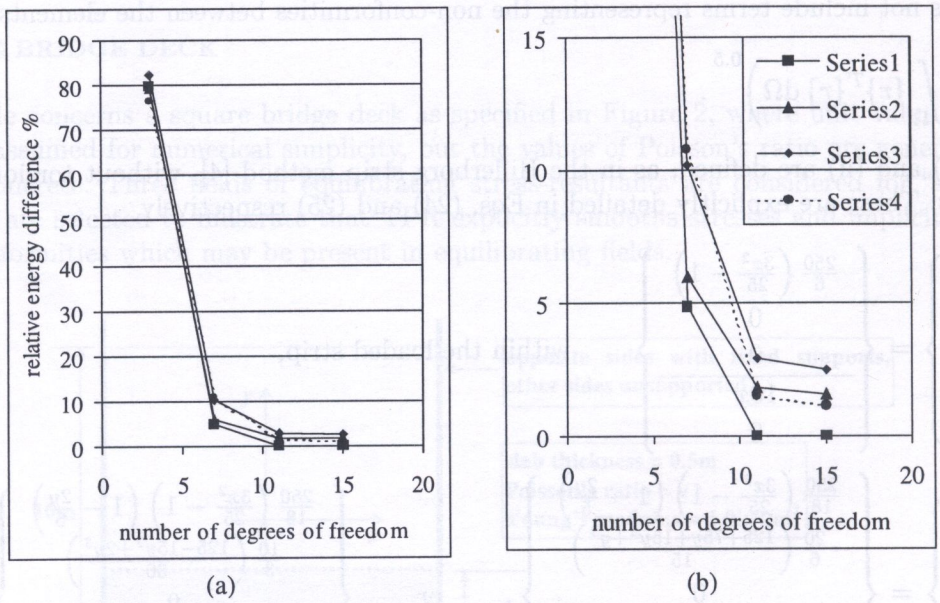


**Fig. 4.** Convergence of **E** with increasing degree $n$ of Trefftz polynomials

to boundary tractions in Eq. (5) which do not give rise to singularities in the analytic solution for stress-resultants.

Field (iii) is both discontinuous and non-conforming, but forms a close upper bound to the overall energy of the solution. Comparisons of stress-resultants when $n = 5$ are shown in Figs. 5–9 for the section through the centre of the patch at $x = 5/3$ m. In these Figures, the lines labeled as Series 1 to 3, or 1 to 4 refer to the "analytic" solution; the Trefftz solution; and the finite element solution field (iii). For the latter, dashed lines are used, and two solutions are defined on either side of the section for stress-resultants $m_y$ and $q_y$ due to the discontinuous nature of the finite element solutions.

The following observations are made on the results from the smoothing of the finite element stress-resultants:

- by inspection of Figs. 5–9, the TPR procedure leads towards stress-resultants which are in good agreement with the analytic solution within the interior of the patch. The boundary layer effects are not recovered in this case since the width of this layer is about 0.5 m which is still small compared with the other dimensions of the patch. The finite element model, though based on a rather coarse mesh, appears to provide sufficiently accurate boundary tractions to drive a good Trefftz type internal solution. This performance appears to be consistent with general observations concerning global Trefftz solutions, namely superconvergence in the interior and greatest errors on the boundary, particularly in the corners [5].

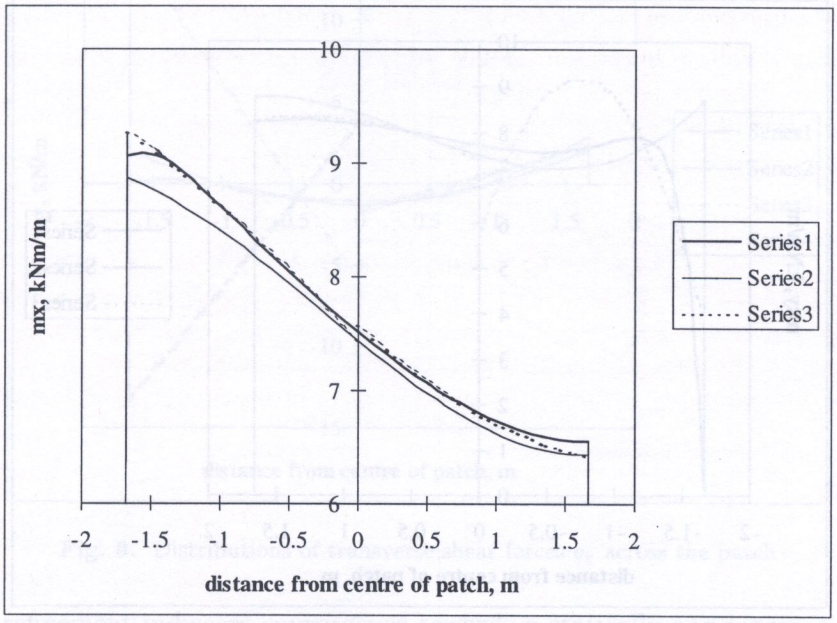


**Fig. 5.** Distributions of bending moment $m_x$ across the patch

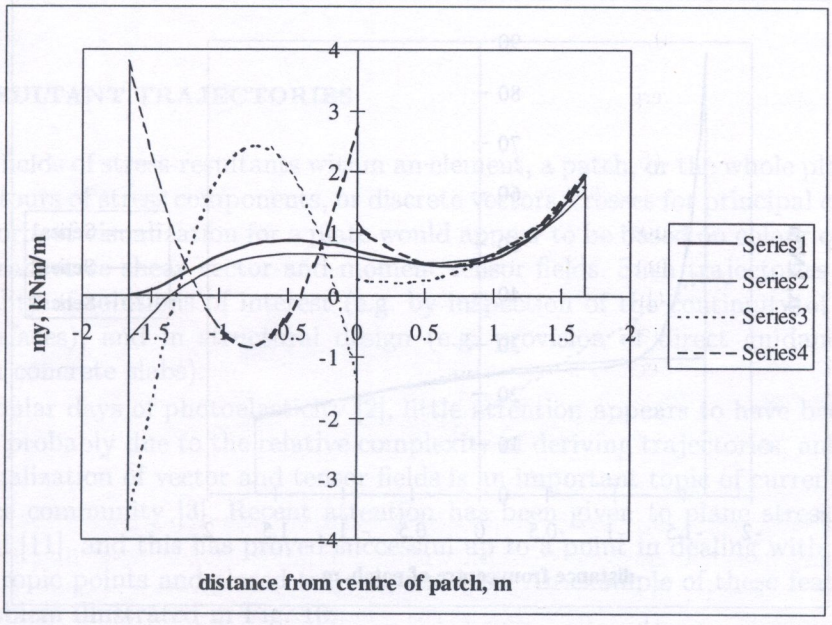


**Fig. 6.** Distributions of bending moment $m_y$ across the patch

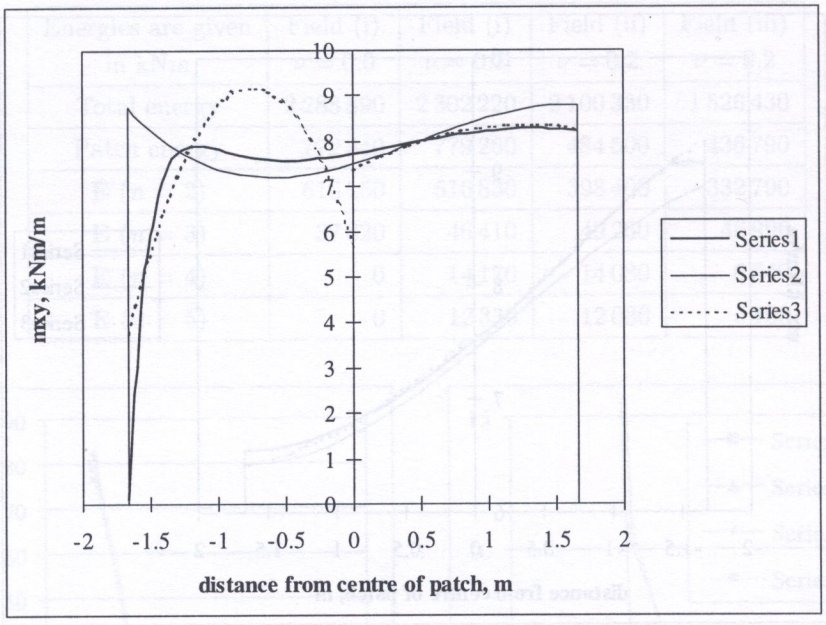


**Fig. 7.** Distributions of torsional moment $m_{xy}$ across the patch

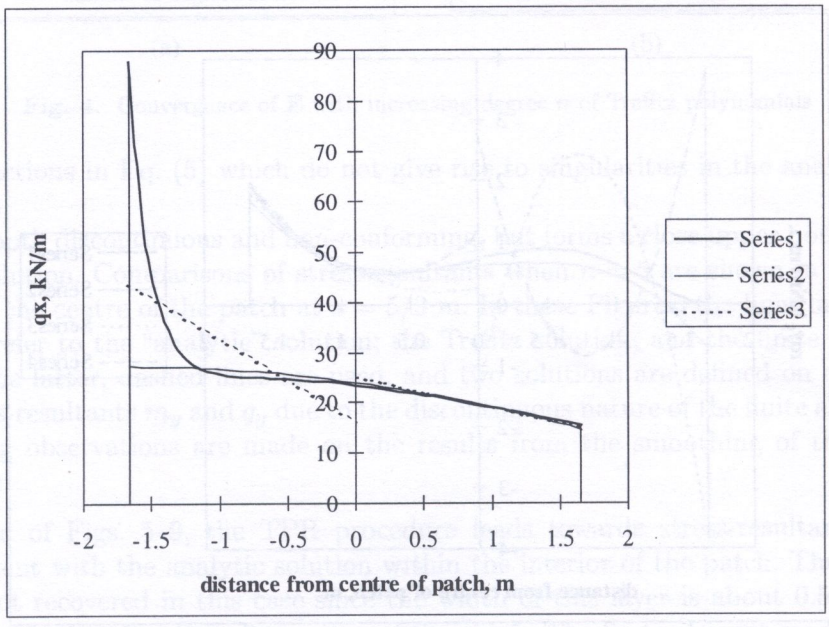


**Fig. 8.** Distributions of transverse shear forces $q_x$ across the patch

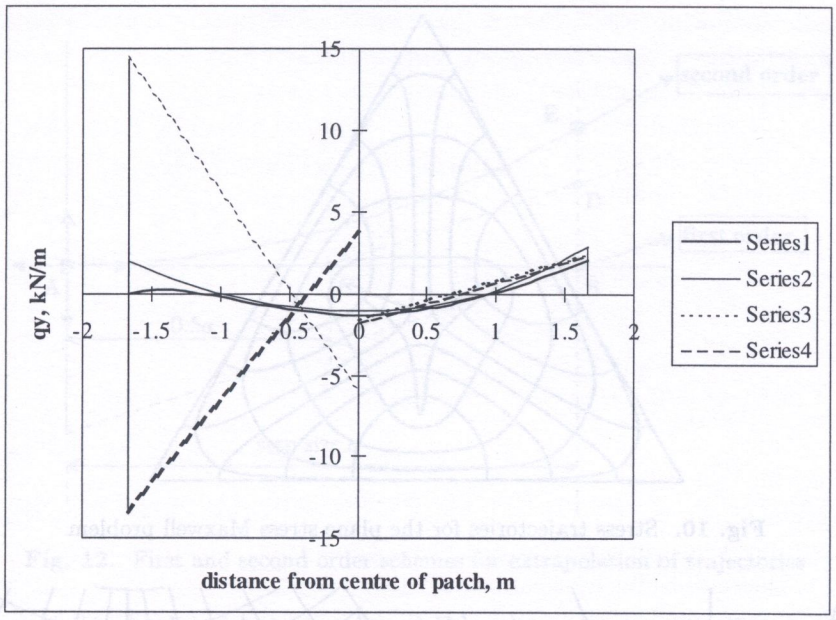


**Fig. 9.** Distributions of transverse shear forces $q_y$ across the patch

- TPR with $p$-refinement indicates convergence towards a statically and kinematically admissible solution which satisfies the traction boundary conditions. These conditions generally imply singularities in the solution due to their discontinuous nature, but such singularities may have little influence towards the centre of a patch.

- since the Trefftz solutions appear to converge towards a conforming one, the quantity $\mathbf{E}$ in Table 3 may be interpreted as a local measure of incompatibility of the equilibrating finite element stress field. In fact if the initial finite element stress field is decomposed as in Eq. (10), then the Trefftz field tends towards $\sigma_c$, and $\mathbf{E} \to \|\sigma_e\|$.

## 5. Stress-resultant trajectories

Visualization of fields of stress-resultants within an element, a patch, or the whole plate, is commonly displayed as contours of stress components, or discrete vectors/crosses for principal components. The most complete form of visualization for a plate would appear to be based on colour coded continuous trajectories of transverse shear vector and moment tensor fields. Such trajectories should assist in judging the quality of solutions of interest (e.g. by inspection of the continuity of tangent vectors at element interfaces), and in structural design (e.g. provision of direct guidance in placing of reinforcement in concrete slabs).

Since the popular days of photoelasticity [2], little attention appears to have been given to such displays. This is probably due to the relative complexity of deriving trajectories, and it is of interest to note that visualization of vector and tensor fields is an important topic of current research in the computer science community [3]. Recent attention has been given to plane stress fields based on an Euler method [11], and this has proved successful up to a point in dealing with the problematic areas where isotropic points and closed trajectories exist. An example of these features is given by the Maxwell problem illustrated in Fig. 10.

Here the stress distribution is hyperstatic, and was caused by the annealing processes of glass manufacture. In this example, the stress field is described by 4th degree polynomials [8], but these are not of the Trefftz type. The increase of degree to 5 has so far proved more demanding, and a successful plot of trajectories is still under investigation.

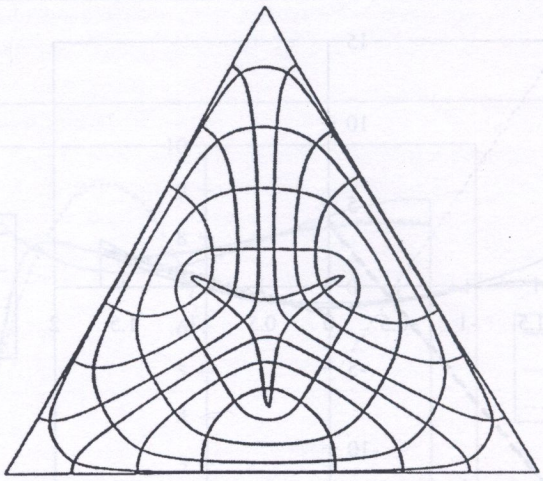

**Fig. 10.** Stress trajectories for the plane stress Maxwell problem

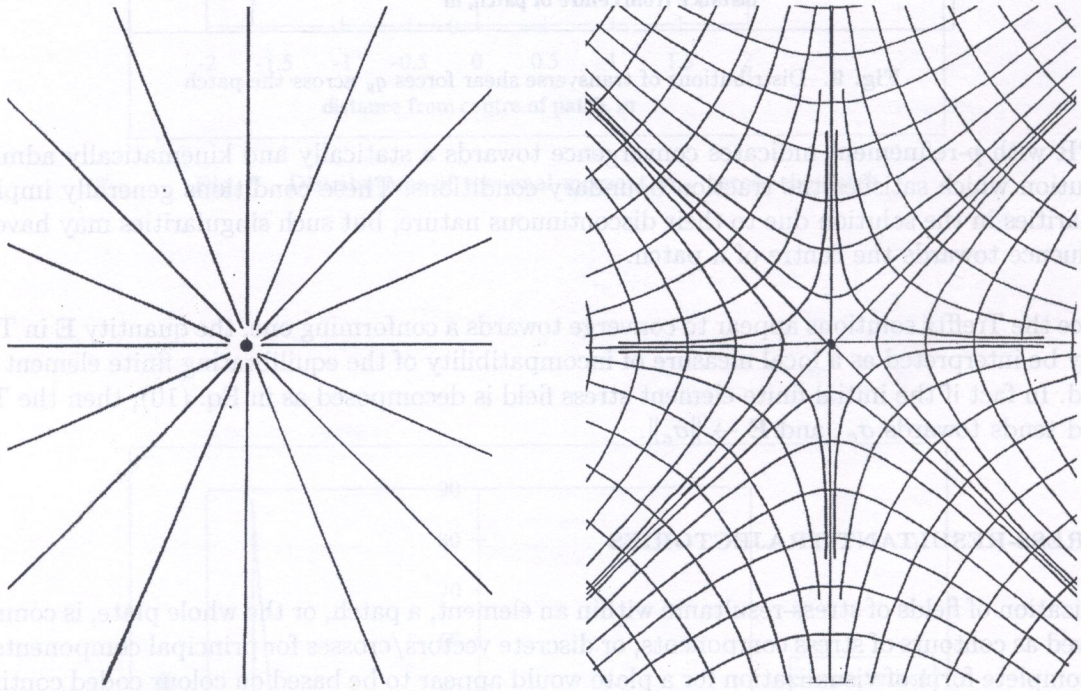

(a) transverse shear force vector (b) moment tensor

**Fig. 11.** Stress trajectories for a Trefftz particular solution for a plate with a uniformly distributed load

A simpler example is based on the particular Trefftz solution given in Eq. (19) for a patch with uniform pressure load. The shear and moment fields are illustrated in Fig. 11 with a single isotropic point at the centre of the patch.

An outline only is here given for a proposed adaptive computational method for plotting trajectories. Extrapolation of trajectories (vector or tensor) is described with the aid of Fig. 12 for first order (piecewise linear, Euler method), and second order (piecewise parabolic, Runge–Kutta method) schemes. From an arbitrary point A, at which the vector/tensor quantity is evaluated, a principal direction (tangent vector) is extended by a step length $a$ to point B. At B the new tangent vector is evaluated, and the Euler method leads to the development of a polygonal trajectory consisting of segments such as AB. A second order scheme seeks the position of point E (EB perpendicular to AB) with the property that the tangent vector at E extends back to the midpoint C

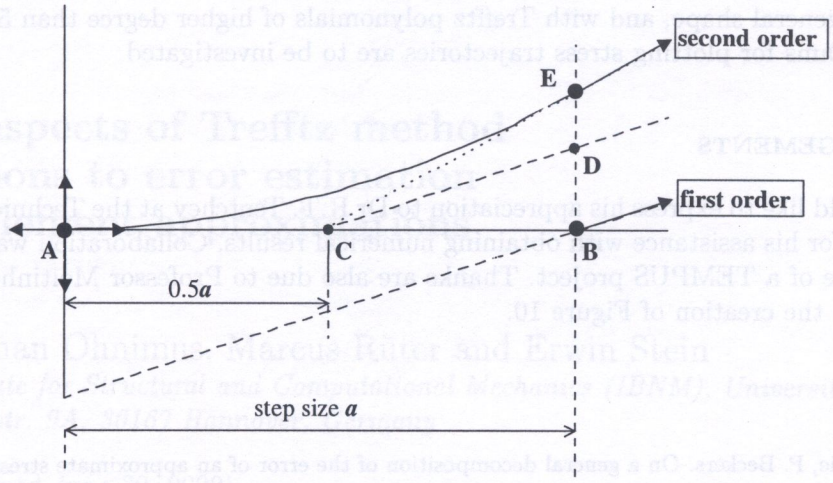


**Fig. 12.** First and second order schemes for extrapolation of trajectories

of AB. A trajectory is interpolated between A and E by the unique parabolic arc with tangents AC and EC at A and E respectively. Point D on BE serves as a starting point in the search for E, where the line DC is parallel to the tangent vector at B.

As with finite element mesh adaptivity, there is the possibility for $h$-refinement — i.e. reduce step length $a$, and/or $p$-refinement — i.e. increase the order of extrapolation.

Such refinements may be required to cope with trajectories having large curvatures, e.g. in the neighbourhood of isotropic points for moments, particularly for the "overlapping" type of point [2] where trajectories can follow a 180° ∪ bend. Another problematic case occurs when trajectories form closed circuits. In such cases numerical errors can lead to the development of a spiral rather than a closed circuit as extrapolated points jump across to adjacent trajectories. The treatment of these cases is currently under investigation.

## 6. Conclusions

- The Trefftz patch recovery process can be formulated so that only boundary integrations are required around a patch.
- The patch equations in effect treat the patch as a hybrid Trefftz type element. This element is by nature hermaphroditic in that it is equally well suited to a stiffness or a flexibility formulation according to the problem to be smoothed.
- When the patch is driven by tractions from an equilibrium finite element model, the $p$-version of the smoothing process tends towards the compatible component $\sigma_c$ of the decomposition of $\sigma_{\mathrm{FE}}$, and the energy of the difference $\mathbf{E}$ between the smoothed stress field and the original finite element stress field tends towards the energy of the self-stressing incompatible component $\sigma_e$.
- In the Reissner–Mindlin plate example, the Trefftz solution appears to converge towards stress-resultants in the patch which can be in close agreement with the analytic solution within the interior of the patch. This indicates that a finite element model based on equilibrium elements and a relatively coarse mesh can provide tractions of sufficient quality to drive a "superconvergent" Trefftz solution in the interior.
- $\mathbf{E}$, as a function of local incompatibility, may serve as a local error indicator. Alternatively the stresses recovered at central nodes of a patch appear to be of good quality and may be used as nodal values in order to define a continuous stress field by interpolation.

- Further work is required to extend the implementation of the concepts to patches bounded by polygons of general shape, and with Trefftz polynomials of higher degree than 5. More sophisticated algorithms for plotting stress trajectories are to be investigated.

## Acknowledgements

The author would like to express his appreciation to Dr R.T. Tentchev at the Technical University of Sofia, Bulgaria for his assistance with obtaining numerical results. Collaboration was made possible as a consequence of a TEMPUS project. Thanks are also due to Professor Moitinho de Almeida of IST, Lisbon, for the creation of Figure 10.

## References

[1] J.F. Debongnie, P. Beckers. On a general decomposition of the error of an approximate stress field in elasticity. *CAMES*, **8**: 261–270, 2001.

[2] M.M. Frocht. *Photoelasticity*, Vol. 1. Wiley, New York, 1941.

[3] H.-C. Hege, K. Polthier, eds. *Mathematical Visualisation Algorithms, Applications and Numerics*. Springer, Berlin, 1998.

[4] A. Hillerborg. *Strip Method of Design*. Viewpoint Publications, Wexham Springs, 1975.

[5] J. Jirousek, A. Venkatesh. A simple stress error estimator for hybrid Trefftz p-version elements. *Int. J. Num. Meth. Engrg.*, **28**: 211–236, 1989.

[6] J. Jirousek, A. Venkatesh. Generation of optimal assumed stress expansions for hybrid-stress elements. *Computers and Structures*, **32**: 1413–1417, 1989.

[7] J. Jirousek, A. Wróblewski, Q.H. Qin, X.Q. He. A family of quadrilateral hybrid-Trefftz p-elements for thick plate analysis. *Comput. Methods Appl. Mech. Engrg.*, **127**: 315–344, 1995.

[8] E.A.W. Maunder, J.P.M. Almeida. Hybrid-equilibrium elements with control of spurious kinematic modes. *CAMES*, **4**: 587–605, 1997.

[9] E.A.W. Maunder, R.T. Tentchev. Hybrid equilibrium models for plate bending based on Reissner–Mindlin theory. *Strojnicky Casopis*, **50**(4): 253–264, 1999.

[10] K.M. Okstad, T. Kvamsdal, K.M. Mathisen. Superconvergent patch recovery for plate problems using statically admissible stress resultant fields. *Int. J. Num. Meth. in Engrg.*, **44**: 697–727, 1999.

[11] O.J.B.A. Pereira, J.P.M. Almeida. Automatic drawing of stress trajectories in plane systems (technical note). *Computers and Structures*, **53**: 473–476, 1994.

[12] O.J.B.A. Pereira, J.P.M. Almeida, E.A.W. Maunder. Adaptive methods for hybrid equilibrium finite element models. *Comput. Methods Appl. Mech. Engrg.*, **176**: 19–39, 1999.

[13] J. Robinson, E.A.W. Maunder. Introduction to the S-adaptivity method. *Finite Elements in Analysis and Design*, **27**: 163–173, 1997.

[14] B. Szabo, I. Babuska. *Finite Element Analysis*. Wiley, New York, 1991.

[15] A. Tessler, H.R. Riggs, M. Dambach. A novel four-node quadrilateral smoothing element for stress enhancement and error estimation. *Int. J. Num. Meth. in Engrg.*, **44**: 1527–1543, 1999.